

# Analytic solutions to the accretion of a rotating finite cloud towards a central object - II. Schwarzschild spacetime

Emilio Tejeda<sup>1\*</sup>, Sergio Mendoza<sup>2\*</sup> and John C. Miller<sup>1,3\*</sup>

<sup>1</sup> *SISSA & INFN, Via Bonomea 265, 34136, Trieste, Italy*

<sup>2</sup> *Instituto de Astronomía, Universidad Nacional Autónoma de México, AP 70-264, Distrito Federal 04510, Mexico*

<sup>3</sup> *Department of Physics (Astrophysics), University of Oxford, Keble Road, Oxford OX1 3RH, UK*

4th February 2021

## ABSTRACT

We construct a general relativistic model for the accretion flow of a rotating finite cloud of non-interacting particles infalling onto a Schwarzschild black hole. The streamlines start at a spherical shell, where boundary conditions are fixed with wide flexibility, and are followed down to the point at which they either cross the black hole horizon or become incorporated into an equatorial thin disc. Analytic expressions for the streamlines and the velocity field are given, in terms of Jacobi elliptic functions, under the assumptions of stationarity and ballistic motion. A novel approach allows us to describe all of the possible types of orbit with a single formula. A simple numerical scheme is presented for calculating the density field. This model is the relativistic generalisation of the Newtonian one developed by Mendoza et al. (2009) and, due to its analytic nature, it can be useful in providing a benchmark for general relativistic hydrodynamical codes and for exploring the parameter space in applications involving accretion onto black holes when the approximations of steady state and ballistic motion are reasonable ones.

**Key words:** accretion, accretion discs, black hole physics, hydrodynamics, relativistic processes

## 1 INTRODUCTION

For several decades, accretion onto black holes has been recognised as the mechanism behind some of the most powerful astrophysical phenomena (see e.g. Frank et al. 2002). It has been extensively studied in the context of Active Galactic Nuclei (AGN) (Genzel et al. 2010), Gamma-Ray Bursts (GRBs) (Piran 2004), X-ray binaries (King 1995), compact binary coalescence (Hughes 2009) and tidal disruption of stars by black holes (Rosswog et al. 2009).

Spherical accretion onto a black hole was found to have low efficiency for converting gravitational potential energy into emitted radiation (Shapiro 1973) and so rotation of the accreting matter has been invoked to give the increased efficiencies required by observations. Rotation in the flow often leads to a centrifugal hang-up with the formation of an accretion disc around the central object through which material inspirals slowly under the action of dissipative mechanisms which can give efficient conversion of gravitational potential energy into radiation. The studies of accretion discs involve many physical inputs including magnetohydro-

dynamic turbulence, the behaviour of highly ionised and degenerate matter, radiative processes and radiation transfer, the formation of strong shocks, nuclear burning, etc; however, gravity and rotation play the dominant role in determining the overall accretion regime and bulk dynamics.

Modern accretion theory began with the pioneering work by Bondi (1952), in which he gave the analytical solution for the steady spherical accretion of an ideal gas cloud onto a central object in Newtonian gravity. The relativistic extension of this was then developed by Michel (1972) who took a Schwarzschild black hole as the central accretor. Rotating inflows were discussed by Prendergast & Burbidge (1968), who introduced the idea of accretion discs which was then developed further by Shakura & Sunyaev (1973) and Novikov & Thorne (1973).

Formation of an accretion disc by infall of a rotating gas cloud onto a central object was first treated by Ulrich (1976) in the context of star formation and accretion discs around protostars. In that Newtonian analysis, the accreting gas was considered to start falling in from a spherical shell located infinitely far away from the central object where it had uniform density. Furthermore, it was assumed that the shell was rotating uniformly and that the fluid elements were following parabolic trajectories. The disc forms

\* E-mail: tejeda@sissa.it (ET), sergio@astro.unam.mx (SM), miller@sissa.it (JCM).

in the plane perpendicular to the cloud's rotation axis as a result of the collision of streamlines coming from mirror-symmetric points on opposite sides of the equator. (See e.g. Cassen & Moosman 1981; Lin & Pringle 1990; Stahler et al. 1994; Mendoza et al. 2004; Nagel 2007, for a clear description of Ulrich's model and the disc formation process.) The relativistic extension of Ulrich's model was investigated numerically by Beloborodov & Illarionov (2001), in relation to wind-fed X-ray binaries, and has also been studied analytically by Huerta & Mendoza (2007) (HM07 hereafter) and Mendoza & Huerta (2008). In the paper to which the present one is a follow-up (Mendoza et al. 2009, - referred to as Paper I in the following), Ulrich's model was extended, within Newtonian gravity, by considering a finite cloud radius and allowing for more general boundary conditions.

In the present paper, we give a full relativistic generalisation of Paper I, studying the stationary inflow of a rotating cloud of non-interacting particles around a Schwarzschild black hole. We shall assume that the particles follow ballistic trajectories and thus, that flow lines correspond to timelike geodesics of Schwarzschild spacetime. Building on previous analytical studies (see e.g. Chandrasekhar 1983), we introduce a novel approach which allows us to describe all of the different types of trajectory with a single analytic expression. The model tracks the infall of particles injected from a finite spherical surface centred on the accretor where the density and velocity distribution of the particles are fixed with wide flexibility. Due to the rotation, a disc-like structure forms in the equatorial plane. In the present work we focus on the accretion flow feeding the disc, and not on the behaviour of matter within the disc itself, where the ballistic approximation certainly breaks down. Our aim is to give an analytic description of this idealised accretion flow, starting far away from the central object and following it down to the vicinity of the equatorial disc, where we then stop our calculations. In the present work, the disc and the black hole are treated just as passive sinks of particles and energy.

In this paper we follow an analytic approach similar to that in HM07, although in Section 7 we show that the final expressions of HM07 need to be modified. Furthermore, in Beloborodov & Illarionov (2001) and HM07 the authors considered as the boundary condition a uniform-density, rigidly-rotating dust shell with all of the fluid elements following parabolic-like motion. In contrast, the present model allows for more general distributions of density, rotation profile, accretion rate and particle energy.

We propose to use this analytic calculation as a benchmark to test the ability of general relativistic hydrodynamical codes in recovering geodesic motion when weakly interacting particles moving on a fixed background metric are considered.

Moreover, the model presented here might also constitute a valuable tool for exploring the effect of different velocity and density distributions on the overall accretion scenario, in astrophysical applications where the ballistic and steady state conditions are reasonable approximations such as supersonic accretion from a wind-fed X-ray binary, as in Beloborodov & Illarionov (2001); sub-Eddington gas accretion onto galactic nuclei (see e.g. Blaes 2007); or collapsing stellar cores, as in Lee & Ramírez-Ruiz (2006) (LR06 hereafter) (see also López-Cámara et al. 2009; Taylor et al. 2011). Exploring the role of different boundary conditions,

before full hydrodynamical simulations are performed, becomes especially useful if one considers that in most of these situations the angular momentum distribution of the accreting matter is highly uncertain, even if it is clear that rotation does play a crucial role in determining the overall accretion efficiency.

As an example of the validity of such an exercise, in Section 6 we compare the velocity and density fields, as predicted by the analytic model, with ones from a roughly equivalent numerical simulation from LR06. In that work, the authors explored numerically the accretion flow of the collapsing interior of a massive star towards a newborn black hole, mimicking relativistic effects by means of a Paczyński & Wiita (1980) pseudo-Newtonian potential.

The structure of our paper is as follows. In Section 2 we present the model and its assumptions. In Section 3, a general expression for the fluid streamlines is given. In Section 4 the velocity fields are described as seen by observers located at infinity and by local observers. Using the continuity equation, a numerical scheme for calculating the density field is developed in Section 5. The model is illustrated with a simple choice of boundary conditions and then compared against a numerical simulation from LR06 in Section 6. In Section 7, we adopt instead the boundary conditions of the Ulrich (1976) model, and give its general relativistic extension. Finally, in Section 8, the non-relativistic limit is considered and the results given in Paper I are recovered.

## 2 MODEL DESCRIPTION

We are interested here in modelling a rotating cloud of particles falling towards a central black hole with mass  $M$ , whose exterior gravitational field is described by the Schwarzschild metric. We assume that the accretion flow has reached a stationary situation characterised by a constant accretion rate  $\dot{M}$ , where from now on, a dot denotes a derivative with respect to the proper time  $\tau$ . Additionally, we assume that the gravitational field of the black hole is the main factor determining the fluid dynamics. We therefore neglect the effects of fluid self gravity, pressure gradients, fluid viscosity, radiation pressure, neutrino capture, etc. In other words, we give a ballistic treatment of the fluid flow.

Consider a cloud subdivided into equal mass fluid elements. We let  $\varrho$  be the matter density and  $n$  be the baryon number density, and introduce an average baryonic rest mass,  $\langle m \rangle$ , such that  $\varrho = \langle m \rangle n$ . We assume that fluid elements are continuously injected from a spherical shell of radius  $r_0$ . This shell represents the outer boundary of the model where the fluid properties are fixed as

$$\varrho_0 = \varrho(r_0, \theta_0, \phi_0), \quad (2.1)$$

$$\dot{r}_0 = \dot{r}(r_0, \theta_0, \phi_0), \quad (2.2)$$

$$\dot{\theta}_0 = \dot{\theta}(r_0, \theta_0, \phi_0), \quad (2.3)$$

$$\dot{\phi}_0 = \dot{\phi}(r_0, \theta_0, \phi_0), \quad (2.4)$$

with  $\dot{r}$ ,  $\dot{\theta}$  and  $\dot{\phi}$  being the radial, polar and azimuthal velocity components, respectively. Figure 1 shows a schematic diagram of the accretion scenario.

We take the four distribution functions in eqs.(2.1)-(2.4) to be differentiable and to be symmetric with respect to the equatorial plane, i.e.

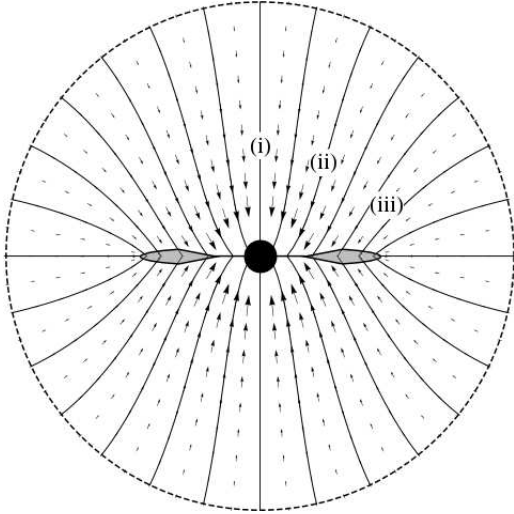


**Figure 1.** Schematic illustration of the present model. Boundary conditions are fixed at a shell with radius  $r_0$  and fluid elements then move along ballistic trajectories. We assume an axisymmetric distribution of angular momentum with its magnitude increasing monotonically towards the equator. The streamlines can be divided into three groups: (i) ones with low angular momentum that accrete directly into the black hole; (ii) ones with intermediate angular momentum which arrive at the equator but do not find a circularisation radius; (iii) ones with large enough angular momentum to be incorporated into an equatorial Keplerian-type accretion disc.

$$f(\theta_0) = f(\pi - \theta_0), \quad (2.5)$$

with  $f = \varrho_0, \dot{r}_0, \dot{\theta}_0, \dot{\phi}_0$ .

Using the boundary distributions for  $\dot{r}_0$  and  $\varrho_0$ , one calculates the total accretion rate as

$$\dot{M} = -r_0^2 \int_0^{2\pi} \int_0^\pi \varrho_0 \dot{r}_0 \sin \theta_0 d\theta_0 d\phi_0. \quad (2.6)$$

Given the ballistic approximation, we have that the specific energy,  $E$ , and the specific angular momentum,  $h$ , are conserved along streamlines. Clearly their actual values vary from line to line and will be distributed in a certain fashion (see eqs. 3.21 and 3.22) as a function of the boundary conditions in eqs. (2.1)-(2.4).

It is a feature of the Schwarzschild spacetime that, for a given mass of the central object and a given streamline, with energy  $E(\theta_0, \phi_0)$ , there exists a critical value of the specific angular momentum,<sup>1</sup>  $h_c$ , such that if  $h(\theta_0, \phi_0) < h_c$  then the corresponding fluid line crosses the black hole horizon (located at  $r_s = 2GM/c^2$ ) before reaching the equatorial plane. On the other hand, for  $h(\theta_0, \phi_0) > h_c$  the streamline reaches the equator and encounters there an equivalent streamline coming from  $(\pi - \theta_0, \phi_0)$ . In a real physical situation one expects that if these collide supersonically then two shock fronts will appear above and below the equator, with the

fluid being incorporated into a disc-like structure. Provided that there is an efficient dissipation mechanism, the shock fronts will remain pinned down to the equator and the disc will remain thin. It is clear that the study of the disc dynamics requires a full hydrodynamical treatment, in which redistribution of angular momentum and energy losses are self consistently taken into account, but such an analysis lies beyond the scope of the present work. Instead, we shall just assume here that an efficient mechanism dissipates all of the kinetic energy associated with the vertical component of the velocity, in such a way that an infinitesimally thin disc forms in the equatorial plane which is then taken to act as a passive energy sink. See López-Cámara et al. (2009) for a full hydrodynamical simulation of a collapsar in which they show that an isothermal disc does indeed remain thin.

In principle one could relax the condition in eq. (2.5) and not assume any particular symmetry for the fluid properties at the boundary. However, in that case we would not have the symmetric collision of streamlines described above. This would lead to formation of a warped disc, making the situation much more complicated.

Following LR06, the streamlines can be divided into three groups depending on the value of their specific angular momentum (see Figure 1): (i) streamlines with low angular momentum, which go directly into the black hole; (ii) streamlines with intermediate angular momentum, which form a small disc within which accretion proceeds on a free-fall time scale (this situation corresponds to the one explored numerically by Beloborodov & Illarionov 2001); (iii) streamlines with larger angular momentum, which have sufficient centrifugal support on their arrival at the equator so that subsequent accretion would occur on a viscous time scale in a Keplerian-type accretion disc.

Now consider the situation in which two neighbouring streamlines start approaching each other in such a way that they would intersect. This type of encounter is qualitatively different from the head-on collision described above, since here, and with a full hydrodynamical treatment, the two approaching streamlines would be prevented from intersecting by the smooth action of pressure forces. It is clear, however, that this cannot be handled within the ballistic approximation and so we must restrict our analysis to distribution functions for which streamlines do not cross before reaching the equator.

Provided that there are no early intersections, then we can use the initial angular position,  $(\theta_0, \phi_0)$ , as a label of the individual streamlines. In the next Section we give an analytic expression for the streamlines that, for any given radius  $r$ , constitutes a mapping  $(\theta_0, \phi_0) \leftrightarrow (\theta, \phi)$ . The condition of no intersection is equivalent to requiring that the Jacobian of this transformation should be non-singular, i.e.

$$J = \left( \frac{\partial \theta}{\partial \theta_0} \right) \left( \frac{\partial \phi}{\partial \phi_0} \right) - \left( \frac{\partial \theta}{\partial \phi_0} \right) \left( \frac{\partial \phi}{\partial \theta_0} \right) > 0. \quad (2.7)$$

While formal, the actual evaluation of this for given boundary conditions is not a trivial task in general. However, if there is axisymmetry it is a sufficient condition that the specific angular momentum should be a non-decreasing function of  $\theta_0$  going from the polar axis to the equator, and that its magnitude should be sufficiently small so that no fluid elements reach a turning point in their trajectories before

<sup>1</sup> Note that taking  $h_c = 2r_s c$  as the critical value, is valid only for streamlines with parabolic-like energies, i.e.  $E = c^2$ .

crossing the equator. For more general cases, it seems best to proceed by trial and error.

### 3 STREAMLINES

Under the ballistic approximation, the streamlines of the accretion model correspond to trajectories of freely-falling test particles (i.e. timelike geodesics) in a Schwarzschild spacetime. In this Section we give a general analytic expression for the spatial projection of these geodesic lines.

#### 3.1 Description in the orbital plane

Let us consider a given fluid element starting to fall in from the point  $(r_0, \theta_0, \phi_0)$ . We denote by  $\mathcal{O}$  the general frame of reference with coordinates  $(t, r, \theta, \phi)$  having its polar axis coinciding with the rotation axis of the cloud.

In a general spacetime, the geodesic equations consist of a second order, non-linear, coupled system of four differential equations. Nevertheless, with the aid of the underlying symmetries of the Schwarzschild spacetime, it is found that the corresponding geodesic equations become separable and reduce to a set of four first order differential equations (see e.g. Frolov & Novikov 1998). A further simplification coming from the spherical symmetry is that the particle motion is confined to a single plane. We denote by  $\mathcal{O}'$  a frame of reference with coordinates  $(t, r, \vartheta, \varphi)$ , especially adapted such that its equatorial plane ( $\vartheta = \pi/2$ ) coincides with the orbital plane.

From the view point of  $\mathcal{O}'$ , the geodesic equation associated with the polar angle becomes  $\dot{\vartheta} = 0$ . This confirms that the whole trajectory stays in a single plane. On the other hand, the equations corresponding to the time and azimuthal coordinates lead to two first integrals of motion, namely the relativistic total specific energy,  $E$ , and the specific angular momentum,  $h$ , defined as:

$$h = r^2 \dot{\varphi}, \quad (3.1)$$

$$E = \left(1 - \frac{r_s}{r}\right) c^2 \dot{t}. \quad (3.2)$$

With the aid of eqs. (3.1) and (3.2) together with the normalisation condition for the 4-velocity<sup>2</sup> ( $u^\mu = dx^\mu/d\tau$ ),  $u^\mu u_\mu = -c^2$ , one gets the following equation governing the proper time evolution of  $r$  for the fluid element

$$\left(\frac{dr}{d\tau}\right)^2 = \varepsilon + \frac{2GM}{r} - \frac{h^2}{r^2} + \frac{r_s h^2}{r^3}, \quad (3.3)$$

where we have introduced the re-scaled energy

$$\varepsilon = \frac{E^2 - c^4}{c^2}. \quad (3.4)$$

<sup>2</sup> Throughout this paper we use Einstein's summation convention with Greek indices running over spacetime coordinates while Latin indices run just over the spatial components.

This definition of energy is convenient because it facilitates comparison with the Newtonian case since, in the non-relativistic limit,  $\varepsilon$  converges to twice the Newtonian total energy.

Since we are interested in a stationary regime, it is convenient to recast the time derivative in eq. (3.3) as a derivative with respect to the azimuthal angle  $\varphi$  ( $d/d\tau = \dot{\varphi} d/d\varphi$ ). Doing this together with the aid of eq. (3.1) allows us to rewrite eq. (3.3) as

$$\frac{dr}{d\varphi} = -\frac{\sqrt{\mathcal{R}(r)}}{h}, \quad (3.5)$$

with

$$\mathcal{R}(r) = \varepsilon r^4 + 2GM r^3 - h^2 (r^2 - r_s r). \quad (3.6)$$

The minus sign in eq. (3.5) is needed because, in the current accretion scenario,  $\varphi$  increases while  $r$  decreases as the fluid elements approach the equator.

Being a fourth degree polynomial,  $\mathcal{R}(r)$  has four roots (with possible multiplicity) and we can write it as

$$\mathcal{R}(r) = \varepsilon (r - r_a)(r - r_b)(r - r_c)(r - r_d). \quad (3.7)$$

Explicit expressions for the roots are given in the Appendix. It is clear that  $r = 0$  is one of them; we treat it in the same way as the others though, since keeping an explicit reference to it allows us to give a general expression for the streamlines. Given that one root is zero, then necessarily at least one other root must be real. The remaining two roots can either also both be real, or can form a complex conjugate pair.

After some analysis of  $\mathcal{R}(r)$  (see, e.g. Mielnik & Plebanski 1962) it follows that if  $\varepsilon < 0$ , all of its real roots are non-negative, while for  $\varepsilon > 0$ , there is exactly one negative root. For  $\varepsilon = 0$ , one of the roots has diverged to infinity and  $\mathcal{R}(r)$  reduces to a third order polynomial. This case is treated in further detail in Section 7.

From eq. (3.5) it is clear that the radial motion is restricted by the condition  $\mathcal{R}(r) > 0$  and so  $r$  is either bracketed in between two consecutive real roots<sup>3</sup> (bounded motion) or is unbounded above.

Let  $r_a$  be the lower bound (periastron). (This includes the possibility  $r_a = 0$ , which corresponds to a plunge orbit.)

If the four roots are real and the motion is upper bounded, we let  $r_b$  be the upper bound (apastron), while for unbounded motion, we let  $r_b$  be the only negative root. We then take the two remaining roots,  $r_c$  and  $r_d$ , such that  $r_c \leq r_d$ .

If two of the roots are complex, we call those roots  $r_b$  and  $r_c$ , with  $r_b = r_c^*$ , and let  $r_d$  be the remaining real root. This case, with complex roots, represents the purely-relativistic ‘‘capture’’ type of orbit, for which particles with non-vanishing angular momentum do not have strong

<sup>3</sup> Whenever these bracketing roots are positive, they correspond to turning points for which the radial velocity vanishes and the particle goes from moving inwards to moving outwards, or vice versa.

enough centrifugal support to prevent them from falling directly into the black hole.

We set the origin of  $\varphi$  at the periastron of the orbit, i.e.,  $r(\varphi = 0) = r_a$ . The solution of eq. (3.5) is then equivalent to finding solutions to the following quadrature problem:

$$\int_{r_a}^r \frac{dr'}{\sqrt{\mathcal{R}(r')}} = -\frac{\varphi}{h}. \quad (3.8)$$

This integral is solvable in terms of Jacobi elliptic functions, as has been discussed several times in the literature (see, e.g. Hagihara 1930; Darwin 1959; Mielnik & Plebanski 1962; Metzner 1963; Chandrasekhar 1983; Miró Rodríguez 1987). These works have followed several different approaches, focusing on different aspects of the solution and using different notations. Labelling the roots in the way described above enables us to give a novel description of the different types of trajectory by means of a single analytical expression, which summarises the results found in the previous work:

$$r = \frac{r_b(r_d - r_a) - r_d(r_b - r_a)\text{cn}^2(\xi, k)}{r_d - r_a - (r_b - r_a)\text{cn}^2(\xi, k)}, \quad (3.9)$$

with

$$\xi = \frac{\sqrt{\varepsilon(r_a - r_c)(r_d - r_b)}}{2h} \varphi, \quad (3.10)$$

where  $\text{cn}(\xi, k)$  is a Jacobi elliptic function with modulus  $k$  given by

$$k = \sqrt{\frac{(r_b - r_a)(r_d - r_c)}{(r_d - r_b)(r_c - r_a)}}. \quad (3.11)$$

Note that, though general, the expressions in eqs. (3.9)-(3.11) should be handled with care in two particular cases: when complex roots are involved and when  $\varepsilon \rightarrow 0$ . In the first case, some intermediate terms will be complex quantities even though the final result will always be a real number. In the Appendix we give alternative expressions for this first case, while the second case is discussed in Section 7.

### 3.2 Relation between the frames of reference

In this subsection we relate the descriptions made in  $\mathcal{O}$  and in  $\mathcal{O}'$ , noting that, for fixed  $t$  and  $r$ , the Schwarzschild metric (see, e.g. Misner et al. 1973) reduces to that of an ordinary 3-sphere and, hence, basic rotation operations can be performed. The easiest way to relate  $\varphi$  to the angles  $\theta$  and  $\phi$  is by means of introducing the turning point in the polar motion, i.e., a point  $\theta_a$  for which

$$\dot{\theta}(\theta_a) = 0. \quad (3.12)$$

The polar motion of a non-equatorial trajectory is always characterised by two turning points which are symmetric with respect to the equator. That is, if  $\theta_a$  satisfies eq. (3.12) then  $\pi - \theta_a$  does as well. Here we choose  $\theta_a$  in the same hemisphere as  $\theta_0$ .

Noting that the polar axis in  $\mathcal{O}'$  is tilted with respect to

the one in  $\mathcal{O}$  by an angle  $\pi/2 - \theta_a$  and performing a series of rotation operations,<sup>4</sup> one obtains the following relationships

$$\cos(\varphi - \varphi_a) = \frac{\cos \theta}{\cos \theta_a}, \quad (3.13)$$

$$\cos(\phi - \phi_a) = \frac{\cot \theta}{\cot \theta_a}. \quad (3.14)$$

Differentiation of eqs. (3.13) and (3.14) with respect to the proper time gives

$$\dot{\varphi} = \frac{\sin \theta \dot{\theta}}{\sqrt{\cos^2 \theta_a - \cos^2 \theta}}, \quad (3.15)$$

$$\sin \theta \dot{\phi} = \frac{\sin \theta_a \dot{\theta}}{\sqrt{\cos^2 \theta_a - \cos^2 \theta}}. \quad (3.16)$$

Evaluating eq. (3.16) at  $\theta_0$  gives the following expression for  $\theta_a$  in terms of known quantities

$$\sin \theta_a = \frac{\sin^2 \theta_0 \dot{\phi}_0}{\sqrt{\dot{\theta}_0^2 + \sin^2 \theta_0 \dot{\phi}_0^2}}. \quad (3.17)$$

From this last equation it is clear that if  $\dot{\theta}_0 = 0$  then  $\theta_a = \theta_0$ .

On the other hand, evaluation of eqs. (3.13) and (3.14) at  $(\theta_0, \phi_0)$  allows us to calculate  $\varphi_a$  and  $\phi_a$  through

$$\varphi_a = \varphi_0 - \cos^{-1} \left( \frac{\cos \theta_0}{\cos \theta_a} \right), \quad (3.18)$$

$$\phi_a = \phi_0 - \cos^{-1} \left( \frac{\cot \theta_0}{\cot \theta_a} \right), \quad (3.19)$$

where, from eqs. (3.9) and (3.10),

$$\varphi_0 = \frac{-2h}{\sqrt{\varepsilon(r_a - r_c)(r_d - r_b)}} \times \text{cn}^{-1} \left( \sqrt{\frac{(r_d - r_a)(r_b - r_0)}{(r_b - r_a)(r_d - r_0)}}, k \right). \quad (3.20)$$

Using eq. (3.1) and combining eqs. (3.15) and (3.16), we can express  $h$  in terms of the boundary conditions as

$$h = r_0^2 \sqrt{\dot{\theta}_0^2 + \sin^2 \theta_0 \dot{\phi}_0^2}, \quad (3.21)$$

while evaluating eq. (3.3) at  $r = r_0$  allows us to calculate  $\varepsilon$ :

$$\varepsilon = \dot{r}_0^2 - \frac{2GM}{r_0} + \frac{h^2}{r_0^2} - \frac{r_s h^2}{r_0^3}. \quad (3.22)$$

From eqs. (3.21) and (3.22) it is clear that  $h$  and  $\varepsilon$  are functions only of the initial angular position  $(\theta_0, \phi_0)$  (i.e. they depend only on the boundary conditions) and that they are conserved along fluid lines.

The expressions given in this Section constitute a description of the fluid lines as a function of the relatively simple but still general boundary conditions given in

<sup>4</sup> First make a rotation of  $-\varphi_a$  about the  $z$  axis in the  $\mathcal{O}'$  frame, then one of  $\pi/2 - \theta_a$  about the resulting  $y$  axis, followed by one of  $\phi_a$  about the final  $z$  axis.

eqs. (2.1)-(2.4). What one needs to do to use these expressions in practice is as follows: from the boundary conditions find the values of  $\theta_a$ ,  $h$  and  $\varepsilon$  using eqs. (3.17), (3.21) and (3.22), respectively. This determines the coefficients of the polynomial  $\mathcal{R}(r)$ , as given by eq. (3.6), and its roots can then be calculated in the way described in the Appendix. The next step is to find the numerical values of  $k$ ,  $\varphi_0$ ,  $\varphi_a$  and  $\phi_a$  and finally one can make use of eqs. (3.9), (3.10) and (3.13) to track a given fluid element in its descent from  $r_0$  towards the equatorial plane, i.e., as  $\theta$  sweeps from  $\theta_0$  to  $\pi/2$ .

#### 4 VELOCITY FIELD

Using eqs. (3.1)-(3.3) together with eqs. (3.15) and (3.16), one obtains the following expressions for the velocity field

$$u^t = \frac{E}{c^2} \left(1 - \frac{r_s}{r}\right)^{-1}, \quad (4.1)$$

$$u^r = -\sqrt{\varepsilon + \frac{2GM}{r} - \frac{h^2}{r^2} \left(1 - \frac{r_s}{r}\right)}, \quad (4.2)$$

$$u^\theta = \pm \frac{h\sqrt{\cos^2\theta_a - \cos^2\theta}}{r^2 \sin\theta}, \quad (4.3)$$

$$u^\phi = \frac{h \sin\theta_a}{r^2 \sin^2\theta}, \quad (4.4)$$

where the sign in eq. (4.3) is positive for  $0 < \theta < \pi/2$  and negative for  $\pi/2 < \theta < \pi$ .

It is convenient to introduce as well the velocity field as described by a set of local observers, since their measurements correspond to physical intervals of proper distance and proper time. Associated with each local observer one has an orthogonal tetrad of 4-vectors constituting a local Minkowskian coordinate set of basis vectors. Let us denote with a bar, coordinates in the local frame of reference, i.e. let  $u^{\bar{\mu}}$  be the components of the 4-velocity of a fluid element passing by a local observer:

$$u^{\bar{\mu}} = (\gamma c, \gamma \vec{V}), \quad (4.5)$$

where  $\gamma$  is the general relativistic Lorentz factor between the local observer and the fluid element, defined as

$$\begin{aligned} \gamma &= \left(1 - \frac{\vec{V} \cdot \vec{V}}{c^2}\right)^{-\frac{1}{2}} \\ &= \frac{E}{c^2} \left(1 - \frac{r_s}{r}\right)^{-\frac{1}{2}} \end{aligned} \quad (4.6)$$

and where

$$V^{\bar{r}} = \frac{c^2 u^r}{E}, \quad (4.7)$$

$$V^{\bar{\theta}} = \frac{r u^\theta}{\gamma}, \quad (4.8)$$

$$V^{\bar{\phi}} = \frac{r \sin\theta u^\phi}{\gamma}, \quad (4.9)$$

are the components of the three-velocity  $\vec{V}$ .

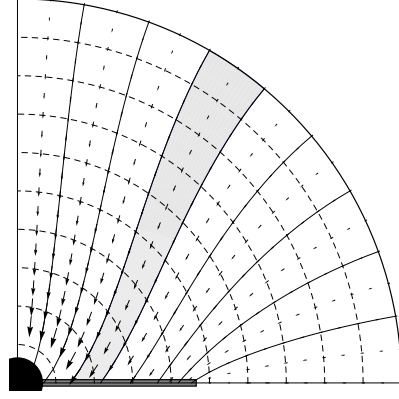


**Figure 2.** Schematic illustration of the construction of a regular grid in  $(\theta, r)$  for calculating the density field. For clarity, the azimuthal direction is not included. The highlighted region constitutes one of the streamline tubes involved in the derivation of eq. (5.6).

#### 5 DENSITY FIELD

The expressions for the streamlines and the velocity field given in Sections 3 and 4 are independent of the value of the density at the boundary and hence the scale for the density can be set arbitrarily. In this Section we derive a numerical scheme for calculating the density field based on the continuity equation. For a general curved spacetime, this equation can be written as

$$\nabla_\mu(n u^\mu) = \frac{1}{\sqrt{-g}} \frac{\partial}{\partial x^\mu} (\sqrt{-g} n u^\mu) = 0, \quad (5.1)$$

where  $g = \det[g_{\mu\nu}]$  is the metric determinant, given in the Schwarzschild case by  $g = -r^4 \sin^2\theta$ . Using the stationarity condition, eq. (5.1) reduces to

$$\frac{1}{r^2 \sin\theta} \frac{\partial}{\partial x^i} (r^2 \sin\theta n u^i) = 0, \quad (5.2)$$

which is simply saying that the spatial divergence of the particle number flux 3-vector  $n u^i$  is zero. We can integrate this equation over a streamline tube, i.e., a volume element consisting of a collection of streamlines coming from an area element  $da|_{r_0}$  at the shell  $r_0$  and ending up at a second sphere with arbitrary radius  $r < r_0$ . Such a streamline tube is illustrated in Figure 2. By means of Gauss's theorem it follows that

$$n u^i da_i|_{r_0} = n u^i da_i|_r. \quad (5.3)$$

The differential area element orthogonal to the radial direction is given by

$$da_r = r^2 \sin\theta d\theta d\phi, \quad (5.4)$$

and so eq. (5.3) can be written as

$$n_0 u_0^r r_0^2 \sin\theta_0 d\theta_0 d\phi_0 = n u^r r^2 \sin\theta d\theta d\phi. \quad (5.5)$$

Using the relation  $d\theta d\phi = J d\theta_0 d\phi_0$ , where the Jacobian  $J$

was given in eq. (2.7), we get the required result for the density field

$$n = \frac{n_0 u_0^r r_0^2 \sin \theta_0}{u^r r^2 \sin \theta J}. \quad (5.6)$$

As long as  $J > 0$ , which means that no intersections of the streamlines occur, and  $u^r < 0$ , which implies that no turning points in the radial motion exist up until the equator is reached, the expression for the density field given by eq. (5.6) is well defined and has no singularities.

The partial derivatives required in the calculation of  $J$  represent a complex computation involving derivatives of an elliptic integral with respect its argument, modulus and integration limit. On the other hand, it is straightforward to evaluate it numerically and so it does not seem worth searching further for a full analytic expression.

We construct a suitable grid for calculating  $J$  in the following way. We start with a homogeneous partition of the initial angles  $(\theta_0, \phi_0)$  and then follow the fluid lines down to the equator in regular radial steps. At every grid point  $(\theta_0, \phi_0, r)$  we store the values of  $\theta$ ,  $\phi$  and  $u^r$  and then calculate  $J$  by means of standard finite differences. Figure 2 illustrates the construction of such a grid.

## 6 EXAMPLE MODEL

Here we illustrate the accretion model presented in the previous sections by applying it with the boundary conditions considered in Paper I, i.e. ones for a uniform shell of matter in uniform rotation:

$$\varrho_0 = \text{const}, \quad (6.1)$$

$$\dot{r}_0 = \text{const}, \quad (6.2)$$

$$\dot{\phi}_0 = \text{const}, \quad (6.3)$$

$$\dot{\theta}_0 = 0. \quad (6.4)$$

This choice leads to several simplifications, the most important being that the accretion flow is then axisymmetric and so, the Jacobian of the angular transformation in eq. (2.7) simplifies to

$$J = \frac{\partial \theta}{\partial \theta_0}. \quad (6.5)$$

From eq. (2.6), we have that the total accretion rate is given by

$$\dot{M} = 4\pi r_0^2 \varrho_0 |\dot{r}_0|, \quad (6.6)$$

and, by substituting the boundary conditions in eqs. (6.1)-(6.4) into eq. (3.21), we get the following distribution of specific angular momentum:

$$h(\theta_0) = h_e \sin \theta_0, \quad (6.7)$$

where  $h_e = r_0^2 \dot{\phi}_0$  is the maximum value of the specific angular momentum, which is reached at the equator of the shell. Since  $\dot{\theta}_0 = 0$ , we have that for every streamline  $\theta_a = \theta_0$ ,  $\varphi_a = \varphi_0$  and  $\phi_a = \phi_0$  giving a simplification of eqs. (3.13)-(3.16). The velocity field is again described by

the expressions given in Section 4 after making the substitution  $\theta_a = \theta_0$ . Regarding the density field, from eqs. (5.6) and (6.5), we find the expression

$$n = \frac{n_0 u_0^r r_0^2 \sin \theta_0}{u^r r^2 \sin \theta} \left( \frac{\partial \theta}{\partial \theta_0} \right)^{-1}. \quad (6.8)$$

Figure 3 shows the projection onto the  $R$ - $z$  plane ( $R = r \sin \theta$ ,  $z = r \cos \theta$ ) of the streamlines, velocity field and density contours for three different combinations of  $\dot{r}_0$  and  $h_e$ . In each case we have set  $r_0 = 20 r_s$ .

For the choice of boundary conditions being used here, the radius of the outer edge of the disc formed as matter reaches the equatorial plane,  $r_D$ , can be calculated from eq. (3.10) and (3.13), taking first  $\theta = \pi/2$  and then  $\theta_0 = \pi/2$ , giving

$$\xi_D = \frac{\sqrt{\varepsilon(r_a - r_c)(r_a - r_b)}}{2 h_e} \left( \varphi_0 + \frac{\pi}{2} \right), \quad (6.9)$$

and then substituting the result into eq. (3.9). In Figure 4, we have plotted  $r_D$  as a function of  $h_e$  as obtained from eq. (6.9) for a fixed value of  $r_0$  and five different values of  $\dot{r}_0$ . Note that  $r_D$  is the radius at which the particle with the largest angular momentum *first* impacts on the equatorial plane; no further motion is then considered. For sufficiently small  $r_D$ , the “disc” will be one within which accretion into the black hole then proceeds on a free-fall time scale, as discussed earlier, and only for larger values of  $r_D$  could it give rise to a Keplerian-type disc. Naturally,  $r_D$  increases monotonically with increasing  $h_e$ , while it decreases with increasing  $|\dot{r}_0|$ . For a given specific angular momentum,  $r_D$  can be substantially smaller when larger values are taken for  $|\dot{r}_0|$ .

Let us now consider boundary conditions corresponding to the collapse of a massive stellar core such as those studied numerically by LR06. In that work, the authors investigated the formation of an inviscid, small-scale accreting disc by making a 2D Smoothed Particle Hydrodynamics (SPH) simulation with relativistic effects being mimicked with a Paczyński & Wiita (1980) (PW) pseudo-Newtonian potential. They included a detailed treatment of neutrino cooling and considered an equation of state with contributions from radiation,  $e^\pm$  pairs,  $\alpha$  particles and free nucleons. We have made comparisons for several of the models discussed in LR06, finding similar results in all cases. For illustration, in Figure 5 we show just one of them, namely the numerical run in which LR06 took a central black hole of  $4M_\odot$  and an external spherical boundary at  $r_0 = 50 r_s$  from which SPH particles were continuously injected with a constant accretion rate of  $\dot{M} = 0.01 M_\odot/\text{s}$ . As radial infall velocity, they took the velocity of free fall from infinity, i.e.  $\dot{r}_0 = -\sqrt{1/50} c$ , and the specific angular momentum of the fluid elements at  $r_0$  was assumed to follow a rigid body rotation distribution with a maximum of  $h_e = 1.9 r_s c$  at the equator of the shell.

The top left panel in Figure 5 shows the accretion flow as calculated from the analytic model, while the top right panel shows a late-time snapshot of the LR06 simulation, taken when a quasi-stationary state had been reached. In general, there is quite good agreement between them until the streamlines have approached the equatorial disc. This is not surprising, bearing in mind that the flow is highly

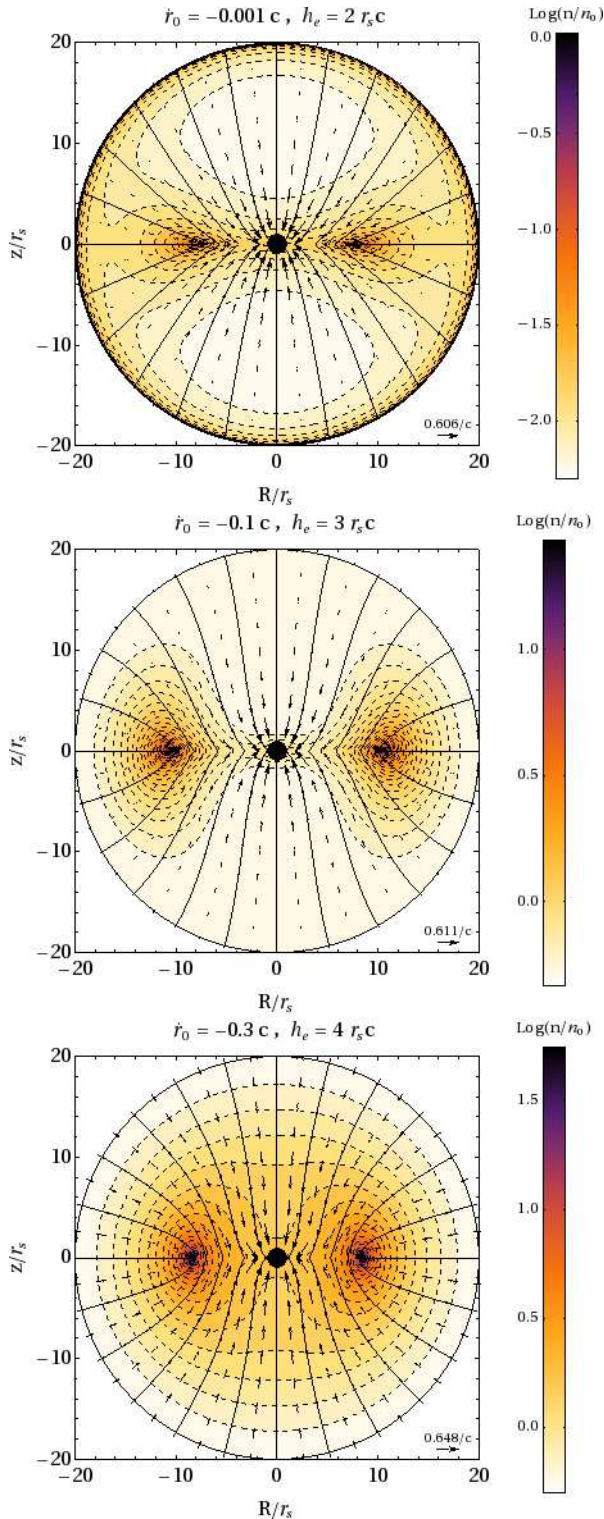


**Figure 3.** Streamlines, velocity field and density contours for different flow parameters. In each of the panels we have taken  $r_0 = 20 r_s$ , while the values of the remaining parameters are indicated in each plot. The plots are projections onto the  $R$ - $z$  plane and the colour coding corresponds to the logarithm of the particle number density,  $\text{Log}(n/n_0)$ . The arrows correspond to the  $V^{\bar{r}}$  and  $V^{\bar{\theta}}$  components of the velocity field.

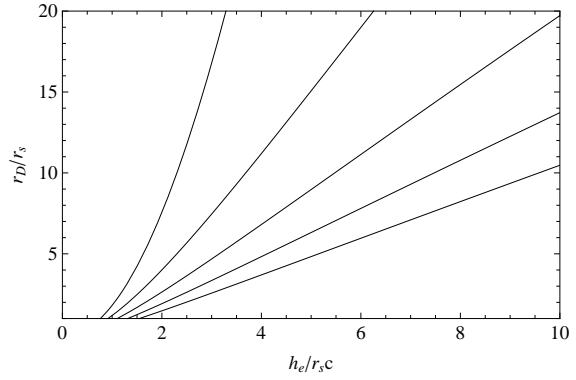


**Figure 4.** The radius of the outer edge of the disc formed as matter reaches the equatorial plane,  $r_D$ , is plotted against the specific angular momentum at the equator,  $h_e$ . A fixed value of  $r_0 = 20 r_s$  is considered. From top to bottom, each curve corresponds to a different inward radial velocity with values  $|r_0|/c = 0, 0.2, 0.4, 0.6, 0.8$  respectively.

supersonic all the way down to the vicinity of the equatorial disc, where strong shocks then appear in the hydrodynamical simulation because of collisions between streamlines coming from opposite points in the two hemispheres. The other four panels present a detailed comparison of the spatial components of the velocity and the density at four spherical cuts. Here, we see very good agreement between the analytical and numerical results for  $u^\theta$  and  $u^\phi$ . For  $u^r$  and  $\varrho$ , there is quite good qualitative agreement, although the numerical results for  $\varrho$  suffer from numerical noise inherent in the interpolation scheme at low particle number densities, and the numerical results for  $u^r$  show higher radial infall velocities, as expected given the use of the PW pseudo-Newtonian potential there, which artificially enhances the radial acceleration.

## 7 RELATIVISTIC EXTENSION OF ULRICH'S MODEL

In this Section we adopt boundary conditions corresponding to the models of Ulrich (1976), Beloborodov & Illarionov (2001) and HM07, i.e. we consider infall from an infinitely large spherical shell of matter with all of the fluid elements having parabolic-like energies ( $r_0 \rightarrow \infty$ ,  $\dot{r}_0 = 0$  and hence  $\varepsilon = 0$ ).

In Ulrich's model, the location of the outer edge of the equatorial disc is simply related to  $h_e$  through

$$r_k = \frac{h_e^2}{GM}. \quad (7.1)$$

In Newtonian gravity,  $r_k$  corresponds to the Keplerian radius of a circular orbit with specific angular momentum  $h_e$  as well as to the semi-latus rectum of a parabolic orbit with this specific angular momentum.

Note that a vanishing initial radial velocity implies  $r_b = r_0$  and, consequently,  $r_c = 0$  while

$$r_{a,d} = \frac{h^2}{4GM} \left[ 1 \pm \sqrt{1 - 4 \left( \frac{r_s c}{h} \right)^2} \right]. \quad (7.2)$$

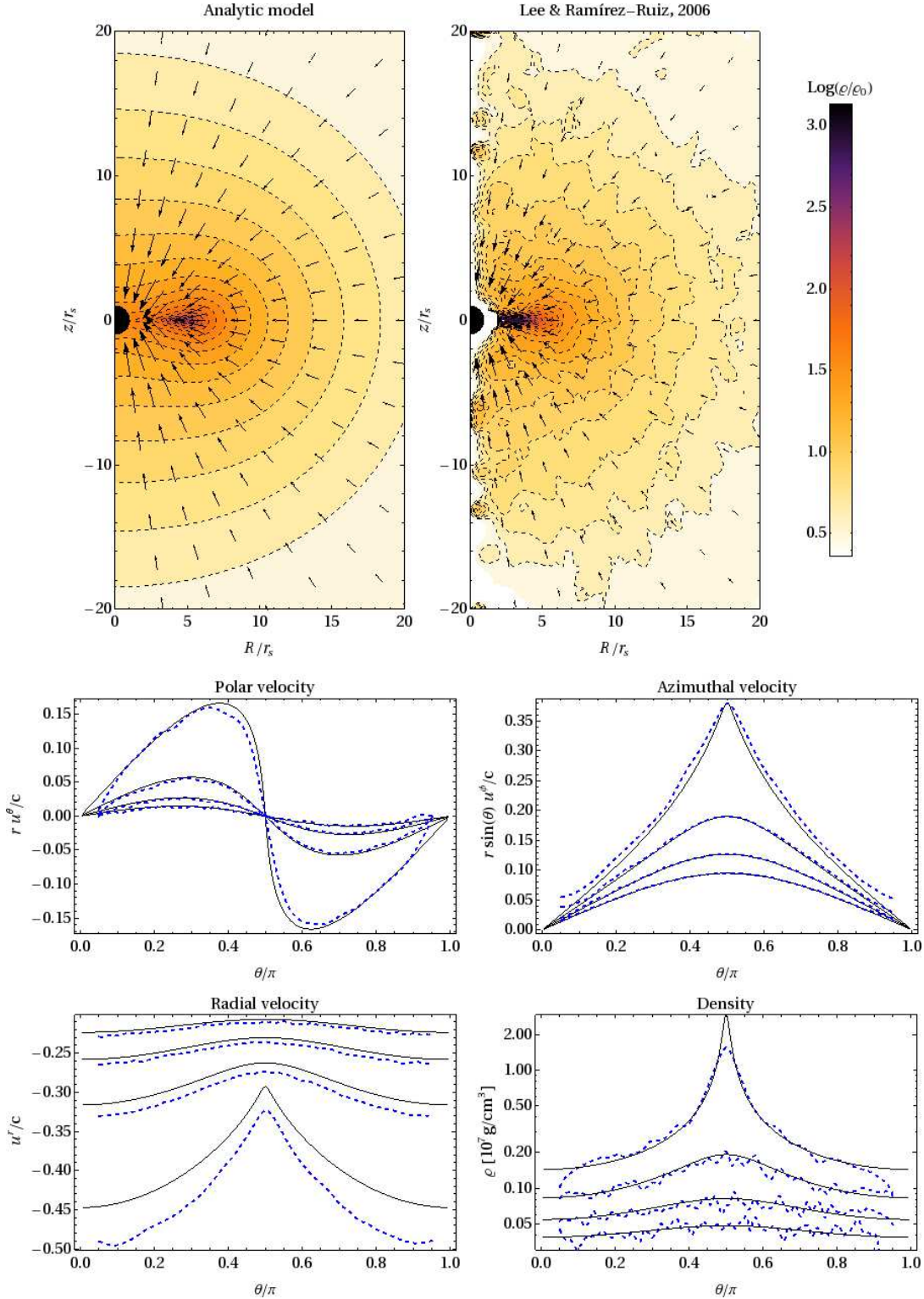


**Figure 5.** Comparison between the analytic model and one of the LR06 simulations. The plots are for an accretion flow towards a black hole with mass  $M = 4M_{\odot}$ , starting from a spherical shell at  $r_0 = 50 r_s$  where the matter density and radial inward velocity are uniform and given by  $\rho_0 = 5.29 \times 10^6 \text{ g/cm}^3$  and  $\dot{r}_0 = -\sqrt{1/50} c = -0.14 c$ , respectively. The specific angular momentum distribution at the shell corresponds to uniform rotation with a maximum of  $h_e = 1.9 r_s c$ . With these boundary conditions, the total accretion rate is  $\dot{M} = 0.01 M_{\odot}/s$ . The top panels show a projection of the accretion flow onto the  $R$ - $z$  plane, together with isodensity contours of the analytic solution (left) and the LR06 numerical simulation (right). The remaining four panels show the velocity components and the density at the radial cuts  $r/r_s = 20, 15, 10, 5$  with the analytic and numerical results being represented by solid and dashed lines respectively.

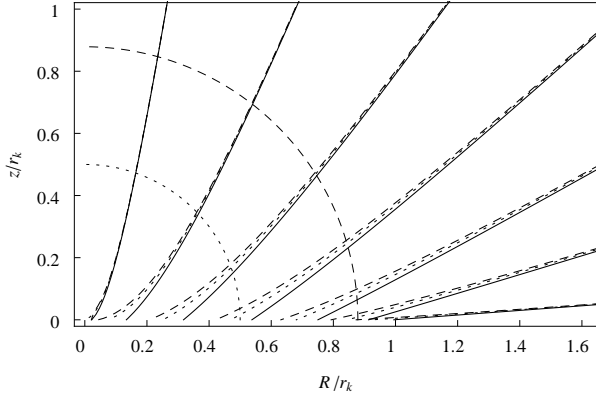


**Figure 6.** Streamlines for the relativistic extension of Ulrich's model ( $r_0 \rightarrow \infty$ ,  $\dot{r}_0 = 0$ ). The continuous line corresponds to  $h_e \gg r_s c$ , i.e. to the non-relativistic limit in which Ulrich's model is recovered. The dotted line corresponds to  $h_e = r_s c$  while the dashed line is for  $h_e = h_c \approx 0.754 r_s c$ , in which case the disc forms entirely inside  $r_s$ , i.e.  $r_D = r_s$ . The quarter-circles correspond the location of the event horizon in each case.

Taking the limit  $r_0 \rightarrow \infty$  in eq. (3.9)-(3.11) and noticing that  $\varepsilon r_0 \rightarrow -2GM$ , one gets the following expression for the streamlines

$$r = \frac{r_a - r_d \operatorname{sn}^2(\xi, k)}{\operatorname{cn}^2(\xi, k)}, \quad (7.3)$$

with

$$\xi = \sqrt{\frac{GM r_a}{2}} \frac{\varphi}{h}, \quad (7.4)$$

$$k = \sqrt{\frac{r_d}{r_a}}. \quad (7.5)$$

Figure 6 shows plots of the streamlines for different values of  $h_e$ . From these, we see how the radius of the equatorial disc decreases as  $h_e$  decreases starting from  $r_D = r_k$  for  $h_e \gg r_s c$  (corresponding to the disc radius in the Ulrich model) down to  $r_D = r_s$  when  $h_e = h_c \approx 0.754 r_s c$ .

HM07 followed an analytic approach similar to the one presented here, but used an incorrect transformation for the polar and azimuthal angles between the systems of reference  $\mathcal{O}$  and  $\mathcal{O}'$ . In particular, eq. (27) in HM07 is not correct and should be substituted by eqs. (3.13) and (3.14) of the present paper.

## 8 NON-RELATIVISTIC LIMIT

In this Section we consider the non-relativistic limit, for which  $h_e \gg r_s c$ . By taking this limit in eq. (3.22), it follows that  $\varepsilon$  becomes equal to twice the total Newtonian specific energy:

$$\varepsilon = \dot{r}_0^2 + \frac{h^2}{r_0^2} - \frac{2GM}{r_0}, \quad (8.1)$$

and, from eq. (3.6), one has that  $r = 0$  is a double root of  $\mathcal{R}(r)$  (i.e.,  $r_c = r_d = 0$ ), with the remaining two roots being real and given by

$$r_{a,b} = \frac{GM}{\varepsilon} (-1 \pm e), \quad (8.2)$$

where  $e = \sqrt{1 + \varepsilon(h/GM)^2}$ .

From eq. (3.11) it follows that  $k = 0$ . For a null value of the modulus, the Jacobi elliptic functions reduce to ordinary trigonometric functions:

$$\operatorname{cn}(x, 0) = \cos(x), \quad \operatorname{sn}(x, 0) = \sin(x), \quad (8.3)$$

and so eqs. (3.9) and (3.10) become

$$\begin{aligned} r &= \frac{r_a r_b}{r_a + (r_b - r_a) \cos^2(\varphi/2)} \\ &= \frac{h^2/GM}{1 + e \cos \varphi}. \end{aligned} \quad (8.4)$$

The second equality in eq. (8.4) is the well-known expression for motion along a conic section with eccentricity  $e$ , representing all of the possible types of orbit in Newtonian gravity.

All of the expressions derived in Section 3.2 concerning the angles  $\varphi$ ,  $\varphi_0$ ,  $\varphi_a$ ,  $\theta$ ,  $\theta_0$  and  $\theta_a$  remain valid, but note that the expression for the initial orbital angle is simplified:

$$\varphi_0 = \cos^{-1} \left( \frac{h^2/GM - r_0}{e r_0} \right). \quad (8.5)$$

The velocity field is given by eqs. (4.2)-(4.4) after taking  $r_s = 0$  and noticing that, within the non-relativistic limit, proper time intervals become identical with coordinate time intervals:  $d\tau = dt$ . The Newtonian results presented in Paper I can be recovered from the expressions given here once the boundary conditions in Section 6 have been adopted.<sup>5</sup> The density field is again given by eq. (6.8). Note that for the particular boundary conditions considered in Paper I, direct evaluation of  $J$  is straightforward and gives the analytic expression presented there.

## 9 SUMMARY AND DISCUSSION

In this paper we have presented an analytic solution for the streamlines of pressureless matter being steadily accreted towards a Schwarzschild black hole. The accretion flow is taken to start from a spherical surface far away from the central mass, with a wide range of boundary conditions being used. The fluid streamlines are then tracked down to the point at which they either become incorporated into a thin equatorial disc or pass inside the black hole event horizon. We have presented a simple numerical algorithm for calculating the density field.

In our model, the fluid streamlines correspond to time-like geodesics of Schwarzschild spacetime. Using Jacobi elliptic functions and some standard identities, we have developed a novel approach for describing all of the different types of trajectory with a single analytical expression.

<sup>5</sup> Note that in Paper I, the azimuthal angle was measured starting from the apastron instead of from the periastron as we do here.

This work extends the Newtonian model presented in Paper I to a general relativistic one in Schwarzschild spacetime and constitutes the analytic solution corresponding to the scenario studied numerically by Beloborodov & Illarionov (2001). We are currently working on the further generalisation of the model to Kerr spacetime. For appropriate boundary conditions, the present solution generalises the classical Ulrich (1976) model and gives corrected expressions for the HM07 model. We have shown that our model recovers the well-known Newtonian expressions in the non-relativistic limit.

Our analytic solution can be used as a benchmark for testing general relativistic hydrodynamical codes. Clearly, such codes should be able to correctly reproduce geodesic motion for a cloud of non-interacting particles in a fixed metric.

Despite the fact that the present model leaves out many physical processes which are relevant for the study of realistic accretion onto black holes, it does include the two main factors determining the bulk dynamics: gravity and rotation. Furthermore, given its flexibility for setting boundary conditions, it can be useful as a computationally inexpensive and efficient tool for exploring the parameter space in applications where the ballistic and steady state hypothesis are approximately valid, such as: sub-Eddington accretion towards a supermassive black hole in a galactic nucleus, wind-fed and Roche-lobe fed X-ray binaries, and collapsar GRB progenitors. In this way one can gain physical insight and get order-of-magnitude estimates of the energy budget before undertaking full-scale simulations. Having such an exploratory tool can be especially relevant if one bears in mind that the parameter domain for many of these systems is vast and often uncertain. An example is the comparison made in Section 6 with the LR06 SPH simulation, where rather good agreement was found between the analytic model and the numerical results.

## 10 ACKNOWLEDGEMENTS

The authors thank Stephan Rosswog for insightful discussions, and are grateful to William Lee for his valuable comments and for providing the LR06 numerical results against which the analytical solution of this paper was compared. ET acknowledges Jorge Moreno for helpful comments on an earlier version of the manuscript. This work was partially supported by a DGAPA-UNAM grant (PAPIIT IN116210-3). SM acknowledges financial support from CONACyT 26344.

## References

- Abramowitz M., Stegun I. A., 1970, *Handbook of Mathematical Functions*. Handbook of Mathematical Functions, New York: Dover, 1970
- Beloborodov A. M., Illarionov A. F., 2001, *MNRAS*, 323, 167
- Blaes O., 2007, in L. C. Ho & J.-W. Wang ed., *The Central Engine of Active Galactic Nuclei Vol. 373 of Astronomical Society of the Pacific Conference Series, Accretion Disks in AGNs*. pp 75–+
- Bondi H., 1952, *MNRAS*, 112, 195+
- Cassen P., Moosman A., 1981, *Icarus*, 48, 353
- Chandrasekhar S., 1983, *The Mathematical Theory of Black Holes*. Oxford University
- Darwin C., 1959, *Royal Society of London Proceedings Series A*, 249, 180
- Frank J., King A., Raine D. J., 2002, *Accretion Power in Astrophysics: Third Edition*. Cambridge University Press
- Frolov V. P., Novikov I. D., 1998, *Black Hole Physics. Basic Concepts and New Developments*. Kluwer Academic
- Genzel R., Eisenhauer F., Gillessen S., 2010, *Rev. Mod. Phys.*, 82, 3121
- Hagihara Y., 1930, *Japanese Journal of Astronomy and Geophysics*, 8, 67
- Hancock H., 1917, *Elliptic Integrals*. New York: Dover, 1917
- Huerta E. A., Mendoza S., 2007, *Revista Mexicana de Astronomía y Astrofísica*, 43, 191
- Hughes S. A., 2009, *Ann. Rev. Ast. & Ast.*, 47, 107
- King A., 1995, in W. H. G. Lewin, J. van Paradijs, & E. P. J. van den Heuvel ed., *X-ray Binaries Accretion in close binaries*. Cambridge University Press, pp 419–456
- Lee W. H., Ramírez-Ruiz E., 2006, *ApJ*, 641, 961
- Lin D. N. C., Pringle J. E., 1990, *ApJ*, 358, 515
- López-Cámara D., Lee W. H., Ramírez-Ruiz E., 2009, *ApJ*, 692, 804
- Mendoza S., Cantó J., Raga A. C., 2004, *Revista Mexicana de Astronomía y Astrofísica*, 40, 147
- Mendoza S., Huerta E. A., 2008, in *Revista Mexicana de Astronomía y Astrofísica Conference Series, Accretion model of a rotating gas sphere onto a Schwarzschild black hole*. pp 18–20
- Mendoza S., Tejada E., Nagel E., 2009, *MNRAS*, 393, 579
- Metzner A. W., 1963, *J. Math. Phys.*, 4, 1194
- Michel F. C., 1972, *Astrophysics and Space Science*, 15, 153
- Mielnik B., Plebanski J., 1962, *Acta Phys. Pol.*, 21, 239
- Miró Rodríguez C., 1987, *Il Nuovo Cimento B (1971-1996)*, 98, 87
- Misner C. W., Thorne K. S., Wheeler J. A., 1973, *Gravitation*. San Francisco: W.H. Freeman and Co., 1973
- Nagel E., 2007, *Revista Mexicana de Astronomía y Astrofísica*, 43, 257
- Novikov I. D., Thorne K. S., 1973, in C. Dewitt & B. S. Dewitt ed., *Black Holes (Les Astres Occlus) Astrophysics of black holes*. Gordon and Breach, New York, pp 343–450
- Paczyński B., Wiita P. J., 1980, *Astronomy and Astrophysics*, 88, 23
- Piran T., 2004, *Reviews of Modern Physics*, 76, 1143
- Prendergast K. H., Burbidge G. R., 1968, *ApJL*, 151, L83+
- Rosswog S., Ramírez-Ruiz E., Hix W. R., 2009, *ApJ*, 695, 404
- Shakura N. I., Sunyaev R. A., 1973, *Astronomy and Astrophysics*, 24, 337
- Shapiro S. L., 1973, *ApJ*, 180, 531
- Stahler S. W., Korycansky D. G., Brothers M. J., Touma J., 1994, *ApJ*, 431, 341
- Taylor P. A., Miller J. C., Podsiadlowski P., 2011, *MNRAS*, 410, 2385
- Ulrich R. K., 1976, *ApJ*, 210, 377

**APPENDIX : SOLUTION OF THE RADIAL EQUATION**

In this appendix we discuss the solution for the radial motion in more detail. Explicit expressions for the roots of the fourth degree polynomial  $\mathcal{R}(r)$  defined in eq. (3.6) are easily given in terms of the following auxiliary quantities (see e.g. Abramowitz & Stegun 1970)

$$Q = (2GM)^2 + 3\varepsilon h^2, \quad (\text{A.1})$$

$$R = (2GM)^3 + 9\varepsilon h^2 \left( GM + \frac{3}{2}r_s \varepsilon \right), \quad (\text{A.2})$$

$$D^2 = R^2 - Q^3. \quad (\text{A.3})$$

When  $D^2 < 0$ , all of the roots are real and are given by

$$r_1 = 0 \quad (\text{A.4})$$

$$r_2 = \frac{2}{3\varepsilon} \left[ \sqrt{Q} \cos \left( \Psi - \frac{\pi}{3} \right) - GM \right], \quad (\text{A.5})$$

$$r_3 = \frac{2}{3\varepsilon} \left[ \sqrt{Q} \cos \left( \Psi + \frac{\pi}{3} \right) - GM \right], \quad (\text{A.6})$$

$$r_4 = \frac{2}{3\varepsilon} \left[ \sqrt{Q} \cos(\Psi + \pi) - GM \right], \quad (\text{A.7})$$

with  $\Psi$  being defined through

$$\cos(3\Psi) = \frac{R}{Q^{3/2}}. \quad (\text{A.8})$$

When  $r_4 < 0$ , we interchange  $r_2$  and  $r_3$  in order to satisfy  $r_2 < r_3$ . In this way, when real, the four roots are ordered as

$$r_1 < r_2 < r_3 < |r_4|. \quad (\text{A.9})$$

On the other hand, for  $D^2 > 0$  two of the roots form a complex conjugate pair. Making the definitions

$$S = \sqrt[3]{D - R}, \quad (\text{A.10})$$

$$T = \sqrt[3]{D + R}, \quad (\text{A.11})$$

the non-zero roots in this case are given by

$$r_{2,3} = \frac{1}{6\varepsilon} \left[ T - S - 4GM \pm i\sqrt{3}(S + T) \right], \quad (\text{A.12})$$

$$r_4 = \frac{1}{3\varepsilon} (S - T - 2GM), \quad (\text{A.13})$$

Since the radial motion is constrained to satisfy  $\mathcal{R}(r) > 0$  then, in the  $D < 0$  case, the radial coordinate is bounded as

$$r \leq r_2, \quad \text{or} \quad r_3 \leq r. \quad (\text{A.14})$$

If the first inequality holds, we write

$$r_a = r_1, \quad r_b = r_2, \quad r_c = r_3, \quad r_d = r_4, \quad (\text{A.15})$$

but, if the second inequality holds, we write

$$r_a = r_3, \quad r_b = r_4, \quad r_c = r_1, \quad r_d = r_2. \quad (\text{A.16})$$

In this way the solution to eq. (3.8) is always given by eq. (3.9).

On the other hand, in the case  $D > 0$ , we take

$$r_a = r_1, \quad r_b = r_2, \quad r_c = r_3, \quad r_d = r_4, \quad (\text{A.17})$$

and once again the expression in eq. (3.9) is a formal solution to eq. (3.8). However, direct evaluation of this involves the use of complex quantities as intermediate steps. It is possible to rewrite eq. (3.9) as an expression involving just real quantities. For doing this, we introduce the following two real constants (having in mind the fact that  $r_1 = 0$ )

$$\alpha = \pm \sqrt{(r_4 - r_2)(r_4 - r_3)}, \quad (\text{A.18})$$

$$\beta = \sqrt{r_2 r_3}, \quad (\text{A.19})$$

where the sign of  $\alpha$  coincides with that of  $\varepsilon$ . We then define

$$\xi_2 = \frac{\sqrt{\varepsilon \alpha \beta}}{h} \varphi = 2\sqrt{\mp k} \xi, \quad (\text{A.20})$$

$$k_2^2 = \frac{(\alpha + \beta)^2 - r_4^2}{4\alpha\beta} = \frac{(1 \mp k)^2}{\mp 4k}, \quad (\text{A.21})$$

where the sign accompanying  $k$  in last equations is the opposite of the one for  $\alpha$ . If we now invoke the following identity for Jacobi elliptic functions (see, e.g. Hancock 1917)

$$\mp k \operatorname{sn}^2(\xi, k) = \frac{1 - \operatorname{cn}(\xi_2, k_2)}{1 + \operatorname{cn}(\xi_2, k_2)}, \quad (\text{A.22})$$

we can rewrite equation (3.9) as

$$r = \frac{\beta r_4 [1 - \operatorname{cn}(\xi_2, k_2)]}{\beta - \alpha - (\alpha + \beta) \operatorname{cn}(\xi_2, k_2)}. \quad (\text{A.23})$$

Note that, in this case,

$$\varphi_0 = \frac{-h}{\sqrt{\varepsilon \alpha \beta}} \operatorname{cn}^{-1} \left[ \frac{\beta r_4 + (\alpha - \beta)r_0}{\beta r_4 - (\alpha + \beta)r_0}, k_2 \right]. \quad (\text{A.24})$$

In summary, the expression for the trajectory of a time-like geodesic in Schwarzschild spacetime can be written as follows:

$$r = \begin{cases} \text{(i)} & \frac{r_2 r_4 \operatorname{sn}^2(\xi, k)}{r_4 - r_2 \operatorname{cn}^2(\xi, k)} \\ \text{(ii)} & \frac{r_4(r_3 - r_2) + r_2(r_4 - r_3) \operatorname{cn}^2(\xi, k)}{r_3 - r_2 + (r_4 - r_3) \operatorname{cn}^2(\xi, k)} \\ \text{(iii)} & \frac{\beta r_4 [1 - \operatorname{cn}(\xi_2, k_2)]}{\beta - \alpha - (\alpha + \beta) \operatorname{cn}(\xi_2, k_2)} \end{cases}, \quad (\text{A.25})$$

$$\xi = \frac{\sqrt{\varepsilon r_3(r_2 - r_4)}}{2h} \varphi, \quad k = \sqrt{\frac{r_2(r_4 - r_3)}{r_3(r_4 - r_2)}}, \quad (\text{A.26})$$

where (i) applies if there are 4 real roots and  $r < r_2$ , (ii) is used for 4 real roots but  $r > r_3$  and (iii) applies when there are just two real roots.